SAND2017-9892J

High Temperature Operation of $Al_{0.45}Ga_{0.55}N/Al_{0.30}Ga_{0.70}N$ High Electron Mobility Transistors

Albert G. Baca , Andrew M. Armstrong, Andrew A. Allerman, Brianna A. Klein, Erica A. Douglas, Carlos A. Sanchez, and Torben R. Fortune
Sandia National Laboratories
Albuquerque, NM 87185, USA

Abstract: AlGaN-channel high electron mobility transistors (HEMTs) are among a class of ultra wide-bandgap transistors that have a bandgap greater than ~ 3.4 eV, beyond that of GaN and SiC, and are promising candidates for RF and power applications. Long-channel $Al_xGa_{1-x}N$ HEMTs with x = 0.3 in the channel have been built and evaluated across the -50°C to +200°C temperature range. Room temperature drain current of 70 mA/mm, absent of gate leakage, and with a modest -1.3 V threshold voltage was measured. A very large I_{on}/I_{off} current ratio, greater than 10^8 was demonstrated over the entire temperature range, indicating that off-state leakage is below the measurement limit even at 200°C. Combined with near ideal subthreshold slope factor that is just 1.3x higher than the theoretical limit across the temperature range, the excellent leakage properties are an attractive characteristic for high temperature operation.

Keywords: Ultra-wide-bandgap; aluminum gallium nitride, power electronics; high electron mobility transistor; HEMT

Introduction

Silicon carbide (SiC) and gallium nitride (GaN) have begun to enable dramatic improvements in the size, weight, and power (SWaP) of power conversion systems [1-5] compared to Si devices. The next generation of semiconductor materials, the so-called "ultra" wide-bandgap (UWBG) materials that have bandgaps larger than that of GaN (E_G > 3.4 eV) will enable the next leap forward in power electronics performance [6]. Although the large bandgaps of GaN and SiC have already suggested their use in emerging radio frequency (RF) and power applications, UWBG devices with even larger bandgaps make them more suited to these applications, particularly in harsh environments, such as at high junction temperatures. In this work we'll describe and characterize emerging UWBG AlGaN-channel high electron mobility transistors (HEMTs) spanning the -50°C to +200°C temperature range.

Transport properties are critically important to transistor operation. Transport properties of AlGaN HEMTs are influenced primarily by the electron mobility, saturation velocity, and the sheet charge present in a quantum well. The latter is quantum-well design dependent and presumed to be comparable among different alloy compositions as long as the conduction band offset is comparable. During high temperature operation, alloy scattering in ternary AlGaN alloys limits the low field mobility relative to binary alloys, e.g. GaN, at temperatures where alloy scattering is dominant (200-400K). At elevated temperatures, beyond room temperature, optical phonon scattering increases considerably and becomes the dominant factor in determining mobility for both binary and ternary alloys. Contrary to the mobility trends with alloy composition, saturation velocity is thought to be comparable in III-N binary and ternary alloys and not extremely temperature sensitive, based on Monte Carlo simulations [7]. This simplified summary of a few key transport properties suggests that AlGaN HEMTs offer possible advantageous operation at high temperature, which coupled with a high critical electric field is advantageous for these devices. Previously published characteristics of AlGaN-channel HEMTs begin to lend support to these motivations [8-13]. In particular, the saturation drain current is reported to be relatively insensitive to temperature in AlGaN-channel HEMTs [9] and very favorable low leakage Schottky gate properties with very high drain current on-to-off ratios have been reported as well [13].

In this work, mid range Al-content for AlGaN-channel HEMTs is explored, and shows considerable improvements in current density at near zero threshold voltage. The HEMTs were also characterized for leakage, subthreshold slope, and other device parameters over temperature. The attractive leakage properties previously attributed to AlGaN-channel Schottky-gated HEMTs are verified to extend to high temperature operation.

Experimental

HEMT samples were grown by metal organic chemical vapor deposition (MOCVD) on Sapphire substrates. The epitaxial structure and HEMT dimensions are defined in Fig. 1, with all layers unintentionally doped. The epitaxial structure consists of an AlN nucleation and buffer layer grown thick enough, 1.6 μm, to planarize on a sapphire substrate. Next a 4.15 μm thick $Al_{0.3}Ga_{0.7}N$ buffer and channel layer was grown and it was followed by a 50 nm $Al_{0.45}Ga_{0.55}N$ barrier layer. The 2-dimensional electron gas (2DEG) resistivity was approximately 3500 Ω/□ from a contactless measurement (not shown), with mercury probe CV measurements indicating a pinchoff voltage near -4.0 V (not shown). Circular, long-channel HEMTs with a gate length of 2 μm, source-gate spacing of 4 μm, gate-drain spacing of 4 μm, and a gate circumference of 330 μm are shown in Fig. 1(b). These devices utilize planar Ti/Al/Ni/Au Ohmic contacts with layer thicknesses comparable to those of GaN/AlGaN HEMTs [14], but temperature optimized for AlGaN channels with a 950°C anneal. Gates utilize Ni/Au Schottky metal deposited into a reactive ion etched opening in a SiN dielectric, with the gate metal partially overlapping the dielectric. Although the HEMT geometry is not compatible with ground-signal-ground pads for RF measurements, some aspects of the device results have implications for RF operation, as will be discussed.

Results

A typical room temperature I_{DS}-V_{DS} plot for the $Al_{0.45}Ga_{0.55}N/Al_{0.3}Ga_{0.7}N$ HEMT is shown in Fig. 2. At the highest gate voltage of +4 V, with a forward biased gate-source diode, the saturation drain current, I_{DS}, is 125 mA/mm with considerable gate current. Biased for negligible gate leakage (up to V_G = +2 V), I_{DS} is 70 mA/mm. Apart from showing good gate control, the I_{DS}-V_{DS} slope is linear through the origin (excepting for gate leakage), indicating good Ohmic contacts [14]. With a threshold voltage (V_{th}) of approximately -1.3 V, this HEMT operates near zero threshold voltage, which with a small adjustment leads to enhancement-mode operation, as required for many power applications. A more negative threshold voltage would lead to higher current density, appropriate for RF applications. Long-channel operation leads to relatively large source-gate and gate-drain spacing, with a low average electric field in the source access region and contributes to present limitations in the HEMT current density. Using the active area dimensions of Figure 1(a) and V_G = +2 V, a specific on-resistance of 4.4 mΩ-cm^2 is calculated.

The threshold voltage of the HEMT is more positive than that implied by the mercury probe CV measurement due to the work function of the Ni/AlGaN interface (compared to the Hg/AlGaN), combined with the effect of possible F ion implantation during the reactive ion etch of the gate opening into the SiN, which has been identified as a method to positively shift V_{th} in AlGaN /GaN HEMTs [15].

Fig. 3 shows the drain (blue) and gate (red) currents as a function of gate voltage on a logarithmic scale. The drain current displays a very steeply decreasing subthreshold current at voltages just below pinchoff and very low levels of leakage current, ~ 10^{-7} mA/mm, for the minimum current levels. The gate current appears instrument limited across the (-10 V) to (+2 V) range. At V_G = +2 V and V_{DS} = 10 V, the local gate-to-2DEG potential doesn't induce a significantly forward biased diode. The subthreshold slope factor of 70 mV/decade approaches the theoretical 60 mV/decade kT/q limit at room temperature. The I_{on}/I_{off} ratio of 8x10^8 is excellent for a Schottky gate device. Hysteresis of the I_{DS}-V_{DS} curves (gate voltage sweep negative vs. positive) was less than 0.1 V.

In order to evaluate the potential of the $Al_{0.45}Ga_{0.55}N/Al_{0.3}Ga_{0.7}N$ HEMT for high temperature operation, the temperature dependence of the drain current is characterized and plotted in Fig. 4. Full *I-V* curves are shown in Fig. 4(a) for the extreme temperatures of -50°C and +200°C and single gate bias *I-V* plots are shown in Fig. 4(b) at all temperatures for V_G = +2 V. The plot colors change gradually from blue to red as the temperature goes from -50°C to +200°C. A trend of decreasing current and *dI/dV* slope with temperature is observed. The I_{DS}-V_{DS} curves of Fig. 4(b) all have a comparable knee voltage (indicated by the vertical arrow) but temperature dependent *dI/dV* slopes (indicated by the slanted arrow) prior to current saturation. The *dI/dV* slopes represent the conductivity from channel resistance, which has contributions from both the sheet resistance and the contact resistance and is analyzed further in the next section.

The temperature dependent subthreshold characteristics of the $Al_{0.45}Ga_{0.55}N/Al_{0.3}Ga_{0.7}N$ HEMTs are shown in Fig. 5. A plot of drain current vs. gate voltage on a logarithmic scale shows that the minimum drain current is invariant with temperature up to 200°C, at V_G smaller than ≅ -2.3 V. Above this voltage, the drain current increases exponentially, with a large subthreshold slope at voltages slightly above ≅ -2.3 V, followed by a lesser subthreshold slope at more positive V_G, and ultimately increases in a manner characteristic of the inclusion of a series connected resistor representing substantial n_s in the 2DEG contributing to the on-state resistance. The inset to Fig. 5 shows that the subthreshold slope is temperature dependent, but also that the threshold voltage shifts negative and then positive over a narrow voltage range with temperature. In addition, a very large I_{on}/I_{off} ratio of over 10^8 is measured at all temperatures up to 200°C.

The room temperature Schottky barrier, ϕ_B = 1.37 eV, was derived from the forward biased I_G-V_{GS} data of Fig. 6 and using an effective Richardson constant from a linear interpolation of the electron effective mass from Schöche *et al.* [16]. A high Schottky barrier compared to that for AlGaN/GaN HEMTs contributes to the excellent leakage properties

Breakdown measurements were carried out and ranged between 190 – 255 V. No further analysis was attempted, except to account for the effect of misalignment in a circular geometry HEMT since the smallest gate-drain dimension likely accounts for the largest electric field sustained prior to breakdown. The minimum L_{GD} dimension is 2.4 μm and the largest average sustained electric field was 80-105 V/μm.

Discussion

$Al_xGa_{1-x}N$ channel HEMTs with a low-to-middle range of x = 0.3 – 0.4 have a number of drawbacks, including insufficiently higher critical electric field, relative to other similar technologies, that may limit their adoption in some applications. Nevertheless, the HEMTs of this study have value as a stepping stone for gaining a better understanding of the entire $Al_xGa_{1-x}N$ alloy composition range. In addition, the HEMTs compare favorably in current density to previous results at a comparable channel composition that is slightly higher at x = 0.38, but also has a slightly more negative V_{th} [8]. Also, the HEMTs of this study all display *I-V* curves that are strictly linear through the origin, evidence of true Ohmic behavior for the source and drain contacts over all temperatures. Such contacts are progressively more difficult to achieve without rectifying behavior as the Al-channel composition is increased [17].

The data of Figures 2-5 indicate that the $Al_{0.45}Ga_{0.55}N/Al_{0.3}Ga_{0.7}N$ HEMTs behave as expected in many respects, but the temperature-dependent characteristics show some distinct advantages relative to competing technologies, as will be described. Figs. 4 and 5 illustrate the drop in I_{DS}-V_{DS} current as temperature increases, in a manner that is similar to that observed in GaN-channel HEMTs [18]. Fig. 5 illustrates that the threshold voltage is relatively consistent, within 0.25 V, indicating that the charge in the 2DEG is relatively constant and that the drain current decrease is due to temperature-dependent transport

properties and not primarily due to V_{th} shift. The vertical arrow of Fig. 4(b) indicates that the knee voltage is relatively invariant over temperature, another indication that the V_{th} is not varying excessively with temperature. The decrease in saturation current is due to the change in initial slope of the I_{DS}-V_{DS} plot and has contributions from both the sheet resistance and the contact resistance.

I_{max} (taken prior to gate turn-on, at V_G = 2 V and V_D = 10 V), I_{DS}-V_{DS} slope (from the data of Fig. 4), and $(R_{sheet})^{-1}$ are plotted as a function of temperature in Fig. 7, after normalizing each parameter to room temperature, 298K. It illustrates the coincident trend of I_{max} to both I_{DS}-V_{DS} slope and $(R_{sheet})^{-1}$ with temperature. R_{sheet} and contact resistivity are analyzed from Ohmic contact transmission line measurements (TLM) [14], which allows the separation of contact resistivity effects from the sheet resistance over temperature.

I_{max} at -50°C is 139% of the 25°C value and at 200°C is 52% of the 25°C value. The 200°C reduction in I_{max} is a somewhat less severe temperature-induced decrease than that for GaN (I_{max} approximates 40% of the room temperature value) [9,18], but considerably greater than that for an $Al_{0.51}Ga_{0.49}N$ channel HEMT (I_{max} approximates 90% of the room temperature value) [9]. The AlGaN-channel HEMTs from this work have quite different I_{max} vs. T behavior than the Tokuda *et al.* paper [9]. A small part of the discrepancy may arise from the expected temperature dependence of mobility, which lessens in magnitude as the Al mole fraction increases [19]. Without understanding to what extent the effect of contact resistivity was accounted for in the Tokuda et al. analysis [9], it is not possible to quantitatively account for the discrepancy.

The plot of Fig. 5 also shows qualitatively that the subthreshold slope factor increases with temperature, as expected, since it is related to kT/q. The subthreshold slope factor is plotted in Fig. 8, and illustrates that it tracks the ideal (dashed line), given by [20-22]

$$S = (kT/q) * \ln(10) * (1 + qD_{it}/C_i) \qquad (1)$$

at temperatures up to 200°C, where q is the electron charge, k is the Boltzman constant, D_{it} is the interface trap density, and C_i is the AlGaN barrier capacitance. The ideal subthreshold slope factor is (kT/q)ln(10) for no interface state charge. From C-V data for C_i, the interface trap density is estimated to be 1×10^{11} cm^{-2}, which compares with $3 - 8 \times 10^{12}$ $cm^{-2}eV^{-1}$ for AlGaN/GaN [21]. This value represents a possibly better interface for the $Al_{0.45}Ga_{0.55}N/Al_{0.30}Ga_{0.70}N$ heterostructure. Since reliable estimates of interface state density may vary widely among different characterization methods, it is possible that the low subthreshold slope factor has another interpretation. Regardless of the best interpretation, a small subthreshold slope factor is desirable so that an e-mode device does not become leaky at elevated temperatures and so that its V_{th} doesn't need to be set unnecessarily high as a remedy for such leakage.

In summary, $Al_{0.45}Ga_{0.55}N/Al_{0.30}Ga_{0.70}N$ HEMTs have been built and characterized over the -50°C to 200°C temperature range. The following near ideal properties of $Al_{0.3}Ga_{0.7}N$-channel HEMTs make them attractive candidates for high temperature operation, where they operate with minimal leakage. The very large, greater than 10^8 I_{on}/I_{off} ratio, the near ideal subthreshold slope factor over the temperature range up to 200°C, and the excellent Schottky gate characteristics contribute to excellent results over temperature. Additionally, the upper temperature of 200°C of this study does not appear to be close to a fundamental limit based on the HEMT leakage properties.

Acknowledgements
This work was supported by the Laboratory Directed Research and Development (LDRD) program at Sandia. Sandia National Laboratories is a multi-program laboratory managed and operated by National Technology & Engineering Solutions of Sandia, LLC (NTESS), a wholly owned subsidiary of Honeywell

Corporation, for the U.S. Department of Energy's National Nuclear Security Administration under contract DE-NA0003525.

References

1. D. K. Schroder, *Int. J. High Speed Elec. Sys.* **21**(1), 1250009 (2012).
2. V. Veliadis *et al.*, *IEEE Elec. Dev. Lett.* **34**(3), 384 (2013).
3. B. J. Baliga, *Semi. Sci. Tech.* **28**, 074011 (2013).
4. M. Su *et al.*, *Semi. Sci. Tech.* **28**, 074012 (2013).
5. M. J. Scott *et al.*, *Semi. Sci. Tech.* **28**, 0774013 (2013).
6. R. J. Kaplar *et al.*, ECS Journal of Solid-State Technology, 6, Q3061 (2017).
7. M. Farahmand, C. Garetto, E. Bellotti, K. F. Brennan, M. Goano, E. Ghillino, G. Ghione, J. D. Albrecht, and P. P. Ruden, *IEEE Trans. Elec. Dev.* **48(3)**, 535 (2001).
8. T. Nanjo, M. Takeuchi, M. Suita, T. Oishi, Y. Abe, Y. Tokuda, and Y. Aoyagi, *Appl. Phys. Lett.* **92**, 263502 (2008).
9. H. Tokuda, M. Hatano, N. Yafune, S. Hashimoto, K. Akita, Y. Yamamoto and M. Kuzuhara, *Appl. Phys. Exp.* **3**, 121003 (2010).
10. N. Yafune, S. Hashimoto, K. Akita, Y. Yamamoto and Kuzuhara, *Jpn. J. Appl. Phys.* **50**, 100202 (2011).
11. T. Nanjo, A. Imai, Y. Suzuki, Y. Abe, T. Oishi, M. Suita, E. Yagyu and Y. Tokuda, *IEEE T. Electron. Dev.* **60**, 1046 (2013).
12. N. Yafune, S. Hashimoto, K. Akita, Y. Yamamoto, H. Tokuda and M. Kuzuhara, *Electron. Lett.* **50**, 211 (2014).
13. A.G. Baca, A.M. Armstrong, A.A. Allerman, E.A. Douglas, C.A. Sanchez, M.P. King, M.E. Coltrin, T.R. Fortune, and R.J. Kaplar, *Appl. Phys. Lett.* **109**, p. 033509 (2016).
14. B. A. Klein *et al.*, to be published
15. Y. Cai *et al.*, *IEEE Electron Device Letters* **26**, 435 (2005).
16. S. Schöche *et al.*, *Applied Physics Letters* **103**, 212107 (2013).
17. E. A. Douglas *et al.*, *Phys. Status Solidi* **A**, 1600842 (2017).
18. R. Menozzi, et al., *IEEE Transactions of Device and Materials Reliability* **8**, 255 (2008).
19. M. E. Coltrin and R. J. Kaplar, J. of Applied Physics **121**, 055706 (2017).
20. S. M. Sze, *"Physics of Semiconductor Devices, 2nd ed.,"* (Wiley Interscience, New York, 1981), p. 463.
21. J. W. Chung *et al.*, *65th Device Research Conference Technical Digest*, (Notre Dame, IN, IEEE, 2007), p. 111.
22. X. Liao *et al.*, Proc. 2014 International Conference on Reliability, Maintainability and Safety, 267 (2014).

Figure Captions:

1. (a) A cross section illustrating the HEMT epitaxial layers and the device structure and (b) a photomicrograph of the HEMT.

2. Room temperature drain current vs. drain voltage for for an $Al_{0.45}Ga_{0.55}N/Al_{0.30}Ga_{0.70}N$ HEMT taken at V_G of 4, 3, 2, 1, 0, -1, and -2 V.

3. Drain current vs. gate voltage for an $Al_{0.45}Ga_{0.55}N/Al_{0.30}Ga_{0.70}N$ HEMT, taken at V_{DS} = 10 V and plotted on a logarithmic scale to highlight the subthreshold characteristics.

4. The temperature dependence of drain current vs. drain voltage for (a) V_G of 2, 1, 0, -1, and -2 V at the temperature extremes of -50°C and 200°C and (b) V_G of 2 V for multiple temperatures between -50°C and 200°C.

5. The temperature dependence of drain current vs. gate voltage for V_{DS} = 10 V. The inset has a magnified scale to better view the Vth and subthreshold slope trends.

6. Room temperature forward biased gate current plot for an $Al_{0.45}Ga_{0.55}N/Al_{0.30}Ga_{0.70}N$ HEMT, consistent with a Schottky barrier height of 1.37 eV.

7. Temperature dependence of I_{max} , I_{DS}-V_{DS} slope, and $(R_{sheet})^{-1}$ for an $Al_{0.45}Ga_{0.55}N/Al_{0.30}Ga_{0.70}N$ HEMT, normalized to room temperature, 298K.

8. Temperature dependence of the subthreshold slope factor for an $Al_{0.45}Ga_{0.55}/Al_{0.3}Ga_{0.7}N$ HEMT.

Figure Captions:

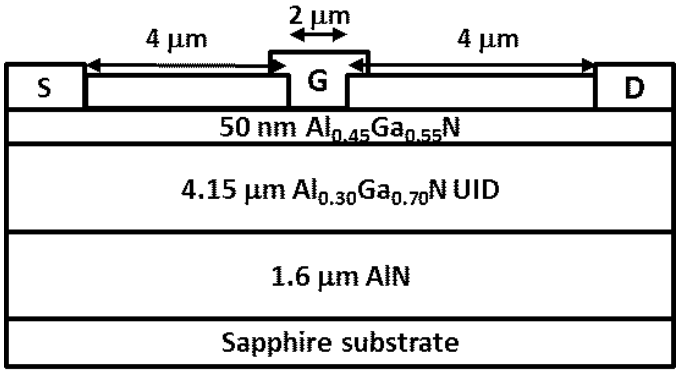

Figure 1(a).

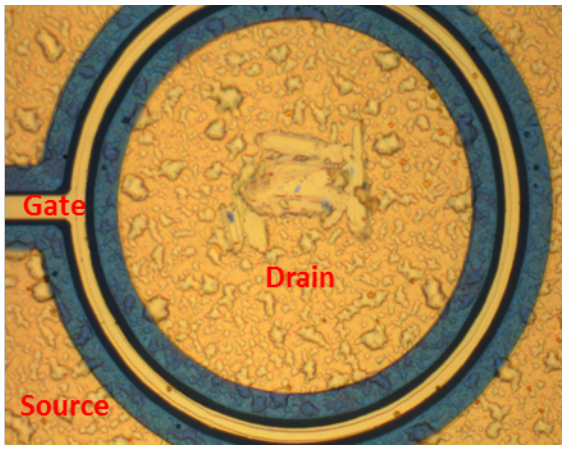

Figure 1(b).

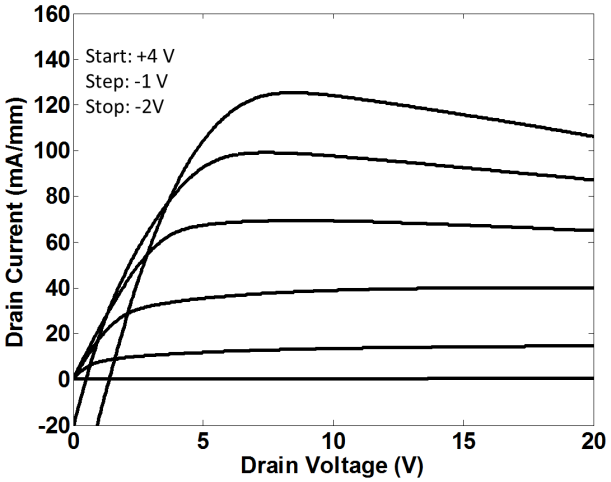

Figure 2.

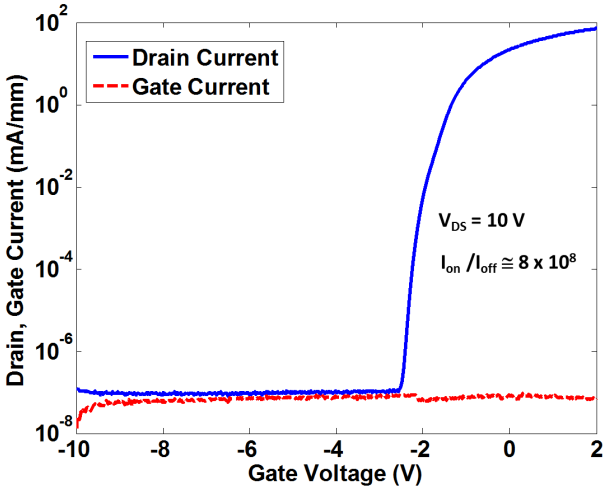

Figure 3.

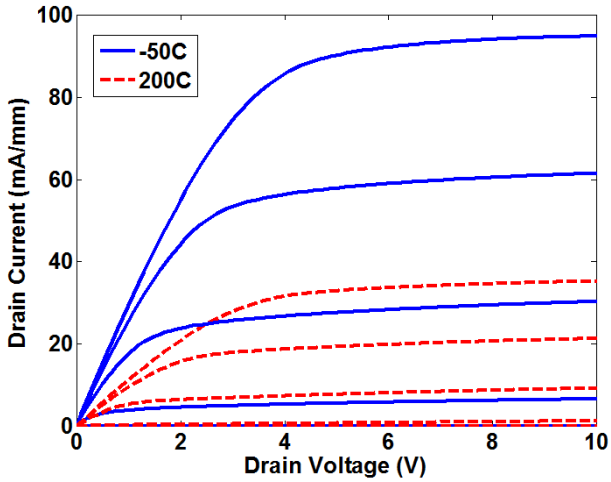

Figure 4(a).

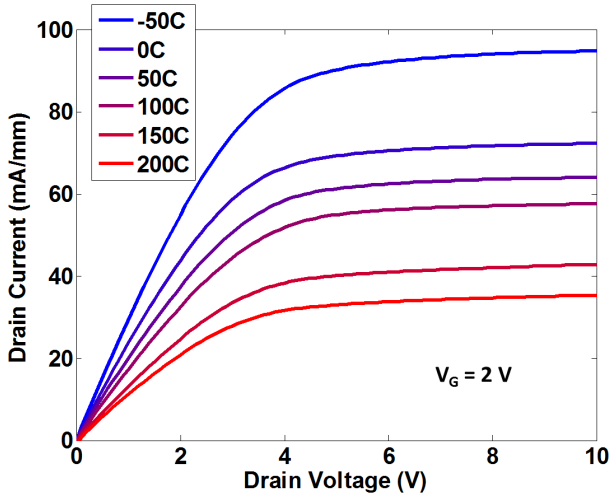

Figure 4(b).

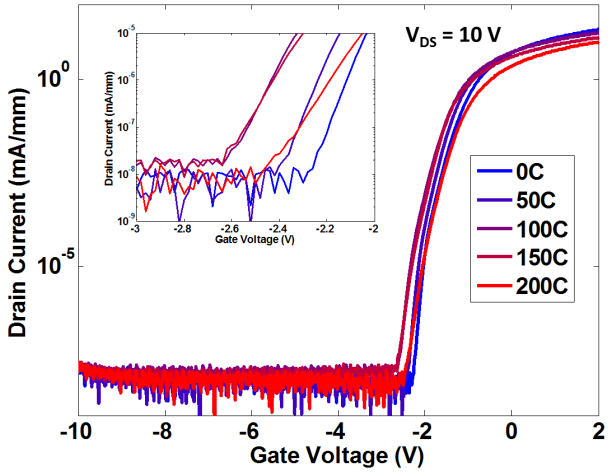

Figure 5.

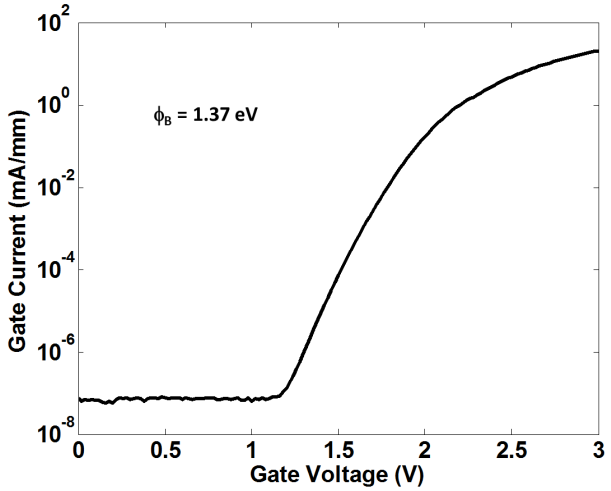

Figure 6.

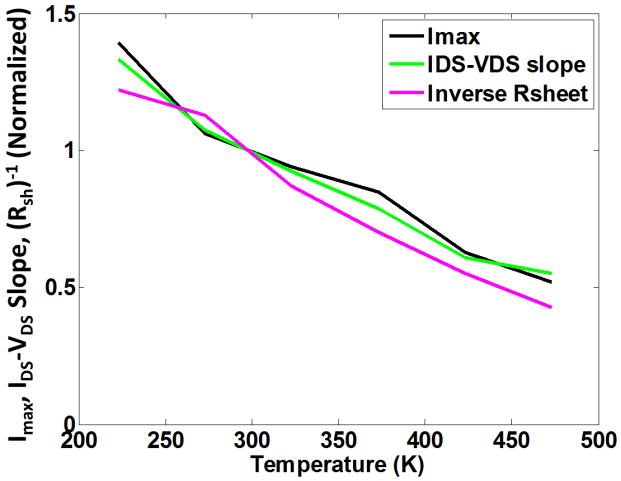

Figure 7.

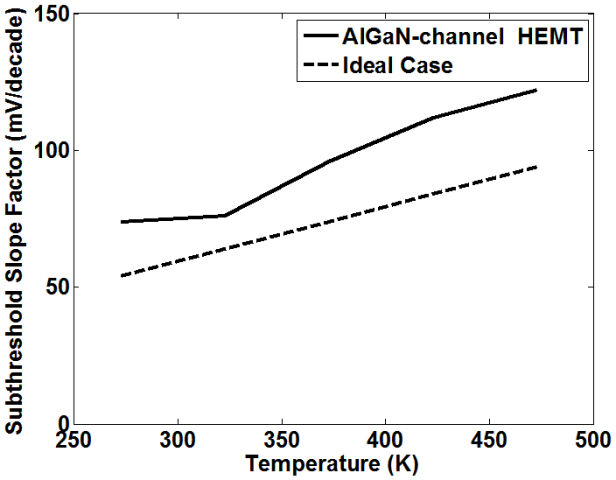
AlGaN-channel HEMT
Ideal Case
Subthreshold Slope Factor (mV/decade)
Temperature (K)
150
100
50
0
250
300
350
400
450
500
Figure 8.